Supporting information

An ultra-stable hafnium phosphonate MOF platform for comparing the proton conductivity of various guest molecules/ions

Yan Huang,[a] Fan Zhou,[a] Jianshen Feng,[c] Hongxia Zhao,[a] Chao Qi,[a] Jinyan Ji,[a] Songsong Bao*[c] and Tao Zheng*[a, b]

[a] School of Environmental and Biological Engineering, Nanjing University of Science and Technology, Nanjing 210094, China

[b] Yangtze River Delta Research Institute, Northwestern Polytechnical University, Suzhou 215400, China

[c] State Key Laboratory of Coordination Chemistry, School of Chemistry and Chemical Engineering, Collaborative Innovation Center of Advanced Microstructures, Nanjing University, Nanjing 210023, China

General considerations. All reagents used in experiments were obtained from commercial resources and used without further purification. All solutions used in experiments were prepared with Millipore water (18.25 MΩ). Hafnium (IV) chloride ($HfCl_4 \cdot nH_2O$) was purchased from Alfa Aesar. Hydrofluoric acid (HF), hydrochloric acid (HCl, 36%), nitric acid (HNO_3, 69%), sulfuric acid (H_2SO_4, 98%), phosphoric acid (H_3PO_4) were purchased from Sinopharm Chemical Reagent Co. Ltd. 1-ethyl-3-methylimidazolium bromide ([EMIm]Br) was purchased from Lanzhou Institute of Physics and Chemistry, Chinese Academy of Sciences. $TppaH_8$ was obtained following the same process reported in our previews word with minor modified treatment.[1]

Synthesis of PHOS-100(Hf). The mixture of $TppaH_8$ (0.0193 g), $HfCl_4$ (0.0242 g), HF (50 μL), and [EMIm]Br (0.3891 g) were added into a 15 mL Teflon–lined stainless steel vessel and heated at 160 °C for three days and then cooled to 25 °C. Colorless block crystals were collected as a pure phase. During the synthesis process, F^- can adjust the reaction kinetics to promote crystal growth and avoid rapid precipitation of amorphous products. For constructing the final structure, F^- ions play the role of terminal coordinated ligands to fill the void coordination sites that cannot be supplied by phosphonates groups.

Crystallographic studies. Single crystal X-ray diffraction data were collected on a Bruker D8-Venture single-crystal X-ray diffractometer equipped with a Turbo X-ray Source (Mo–Ka radiation, λ = 0.71073 Å) adopting the direct-drive rotating anode technique. The raw data of PHOS-100(Hf) was solved by a direct method and refined by SHELXTL.[2] All the atoms were refined anisotropically except hydrogen atoms. The uncoordinated guest molecules in void space were treated by the SQUEEZE command to remove electrons belong to $[EMIm]^+$ and water molecules.[3]

Powder X-ray diffraction. Powder X-ray diffraction patterns were measured on a Bruker D8 advance X-ray diffractometer with Cu–Ka radiation (λ = 1.54056 Å) equipped with a Lynxeye one-dimensional detector. The calculated PXRD pattern in the text comes from low temperature data, while experimental PXRD are collected at room temperature, so there are some differences in the small angel area.

Infrared spectroscopy. Infrared spectra were collected on a Thermo Scientific Nicolet iS50 FT-IR instrument at room temperature.

Thermal stability. Thermogravimetric analysis was performed on a NETZSCH STA 449F3 instrument in the range of 30–600 °C under a nitrogen flow with a heating rate of 10 °C/ min.

Chemical stability. The samples of PHOS-100(Hf) were soaked in aqueous solutions at variable pHs (pH = 1–14, solution of HCl or NaOH) for 24 hours. The samples of PHOS-100(Hf) were soaked in aqua regia, oleum, concentrated HNO_3 and HCl for 12 hours. Then the MOF powders were centrifuged and used for PXRD measurements.

Sample activation and loading. 700 mg PHOS-100(Hf) were soaked in aqueous solutions of 6 M HCl, then put in a centrifuge-tube and shake for two days; the above treatment was repeated three times; then, the samples were washed with water and ethanol and dried in air. The result samples (50 mg) were immersed in the diluted H_2SO_4 (3 M) and H_3PO_4 (3 M), respectively, and then stirred 30 minutes at room temperature. The final acid-loaded samples were obtained by centrifugation and dried in air.

Proton conduction. The four samples are put into a mold with a 2.5 mm radius and compressed under 0.46 Ton pressure to obtain four round pellets. The thickness of samples is measured by a thickness gauge is 0.75, 0.60, 0.57, and 0.62 mm, respectively. Then the pellets were coated with silver glue on the top and bottom, connected to gold wires, and dried in the air. The quasi-four-probe method is used to measure the proton conductivity of the pellets. The prepared samples are ready for Alternating current (ac) impedance analyses. In these measurements, the ac frequency ranges from 0.1 to 10^6 Hz, and the temperature spans from 288 to 323 K; relative humidity (RH) in the range of 45 % and 95 %. The input voltage is 300 mV. The temperature and humidity were set to a certain value and kept for 12 hours before measurements.

Water adsorption and desorption isotherms. Adsorption/desorption isotherms for water vapor were measured with a BELSORP-max instrument (BEL Japan, Inc.). The samples were pretreated at 100 °C under vacuum for 12 hours.

Table S1. Crystal Data and Refinement Details for **PHOS-100(Hf).**

	PHOS-100(Hf)
Formula	$C_{67}H_{56}F_{18}Hf_7O_{24}P_8$
M	3084.31
CCDC No.	2041165
Crystal system	Orthorhombic
Space group	*Cmca*
a / Å	17.594(3)
b / Å	28.869(6)
c / Å	26.289(5)
α / deg	90
β / deg	90
γ / deg	90
V /Å^3	13353(4)
Z	4
ρ_{calcd} / g cm^{-3}	1.534
F (000)	5744
μ(Mo Kα) /mm^{-1}	5.584
GOF on F^2	1.015
$R_1{}^a$, $wR_2{}^b$ [I>2σ(I)]	0.1056, 0.3109
$(\Delta\rho)_{max}$, $(\Delta\rho)_{min}$ / eÅ^{-3}	-5.50, 10.31
R(int)	0.1180

$^{a.}$ $R_1 = \Sigma||F_o| - |F_c|| / \Sigma|F_o|$. $^{b.}$ $wR_2 = [\Sigma w(F_o^2 - F_c^2)^2 / \Sigma w(F_o^2)^2]^{1/2}$

Table S2. Selected Bond Distances (Å) for **PHOS-100(Hf)**.

Hf1-O1	2.050(16)	Hf3-F4	1.95(3)
Hf1-O4A	2.06(2)	Hf3-F5	2.019(18)
Hf2-O2	2.11(2)	P1-O1	1.477(18)
Hf2-O7B	2.21(3)	P1-O2	1.54(2)
Hf2-F1	1.87(4)	P1-O3	1.51(2)
Hf2-F2	1.89(3)	P2-O4	1.53(2)
Hf3-O5C	2.07(2)	P2-O5	1.46(2)
Hf3-O6	2.108(17)	P3-O6	1.480(19)
Hf3-F3	1.90(2)	P3-O7	1.45(3)

Symmetric codes for **PHOS-100(Hf)**: A: 1/2-x, y, 1/2-z; B: -1/2+x, 1/2+y, z; C: 1-x, 1/2-y, 1/2+z;

Figure S1. The molecular structure of ionic liquids.

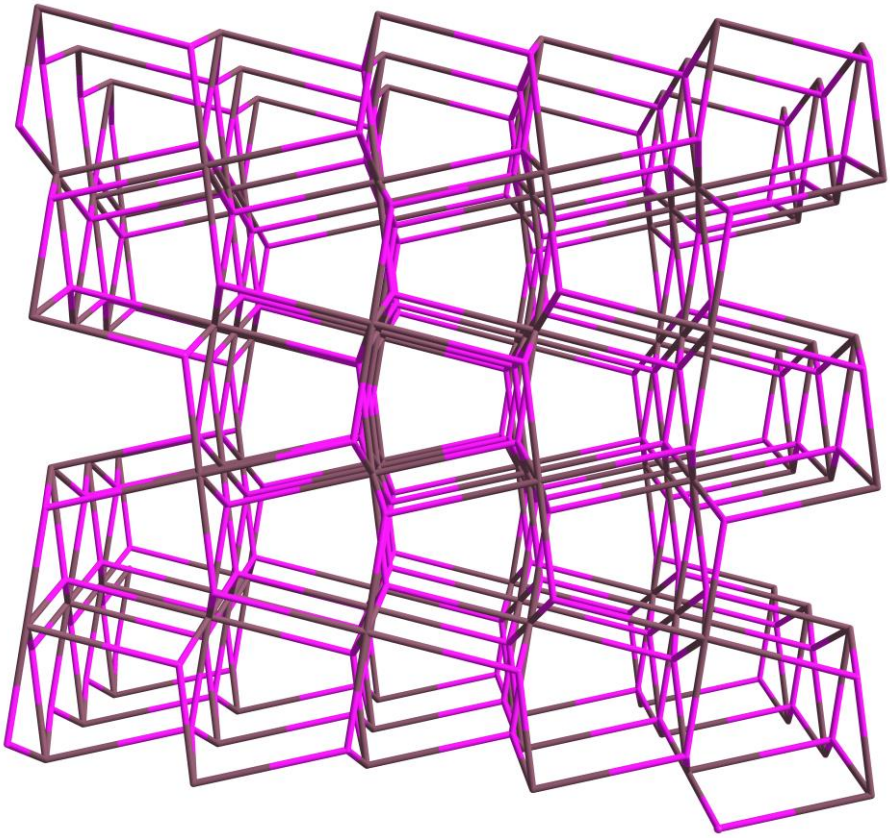

Figure S2. The topological structure of **PHOS-100(Hf).**

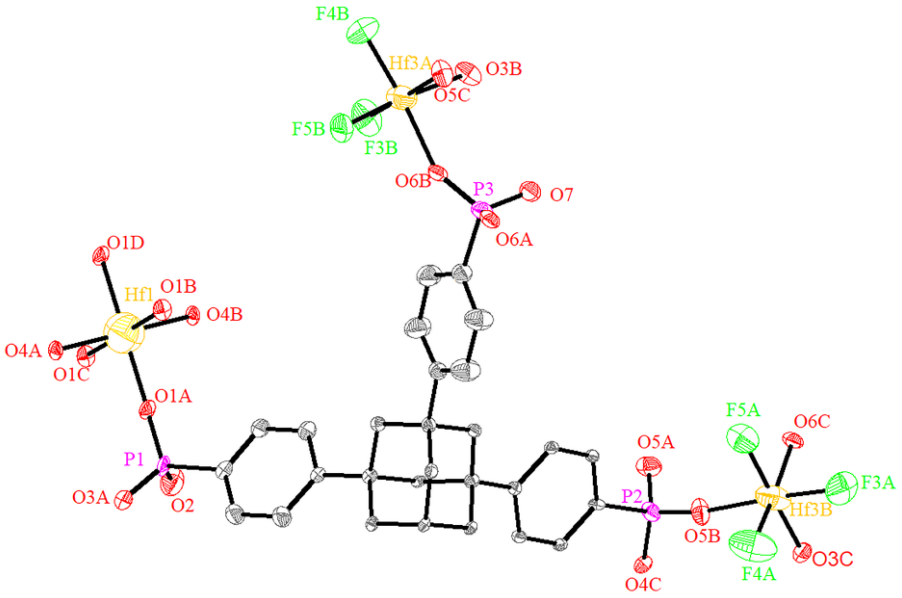

Figure S3. Asymmetric building unit of **PHOS-100(Hf)** with atomic labeling scheme.

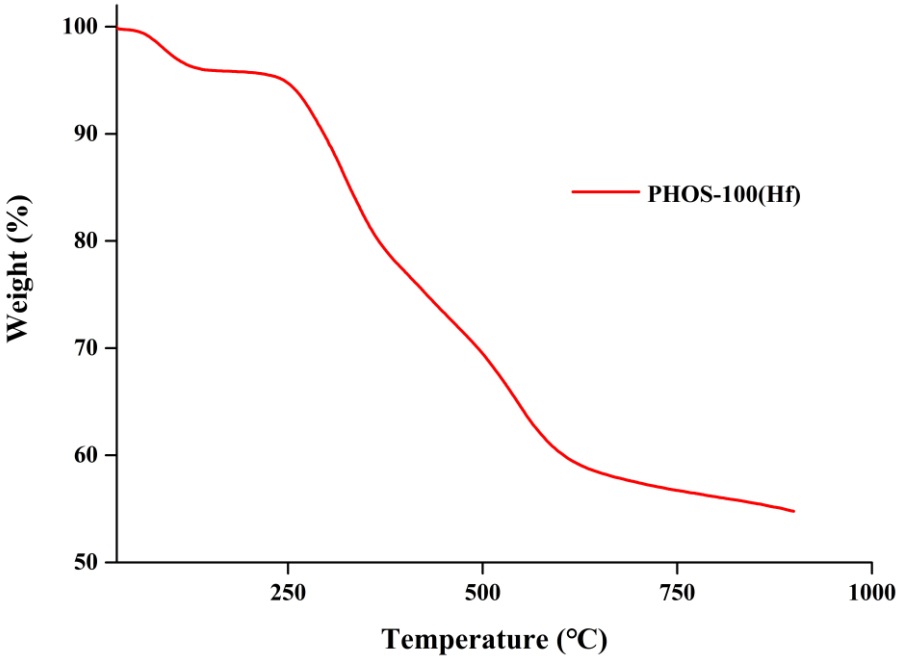

Figure S4. TGA curve of **PHOS-100(Hf).**

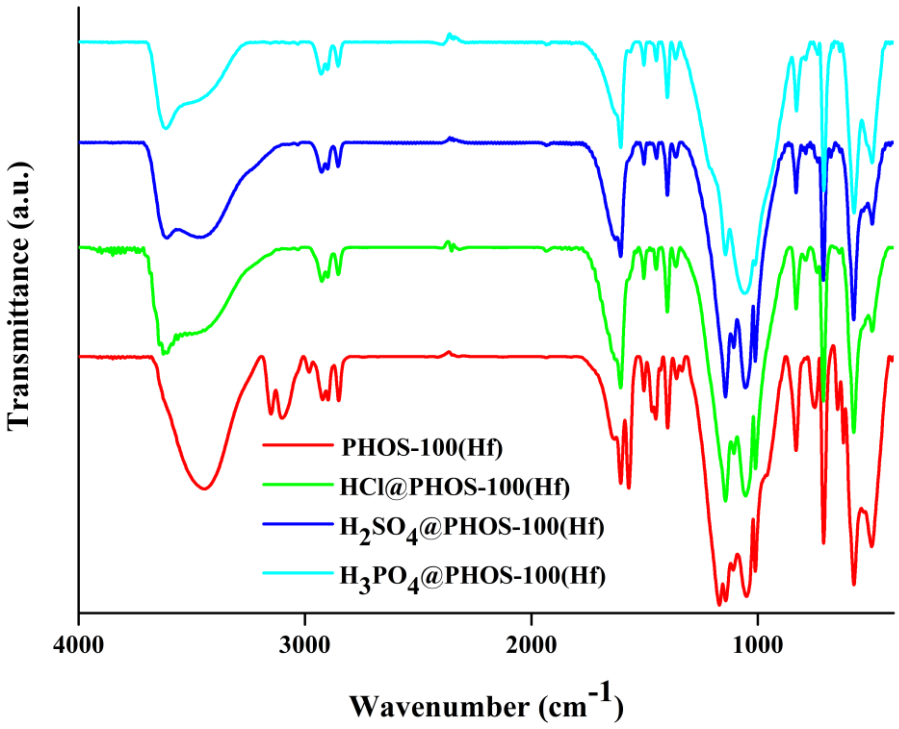

Figure S5. IR spectrum of four samples.

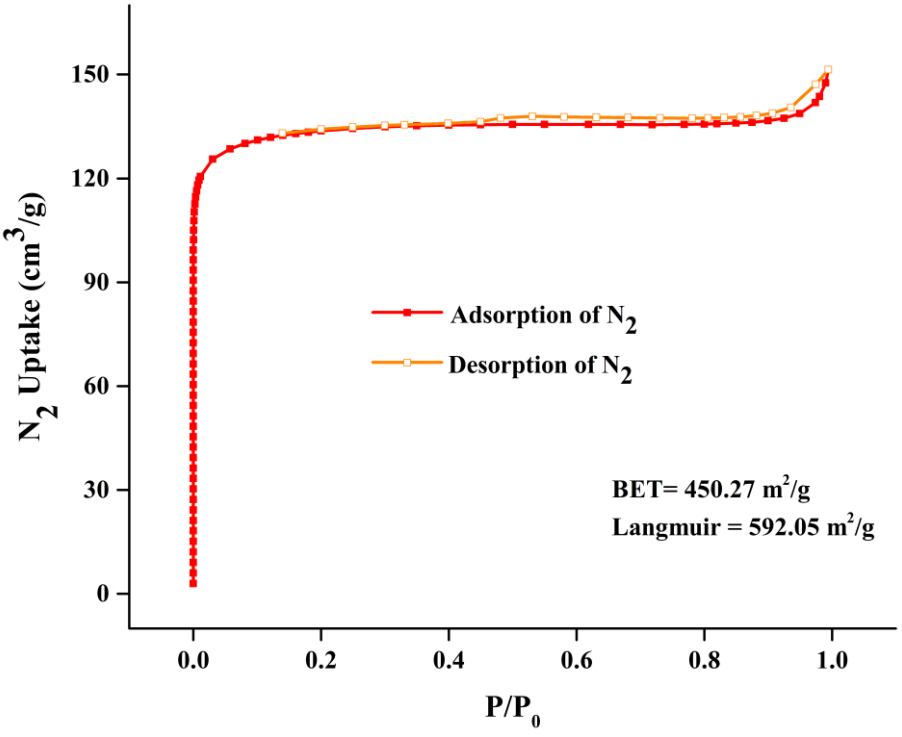

Figure S6. N_2 adsorption and desorption isotherms of **PHOS-100(Hf)**.

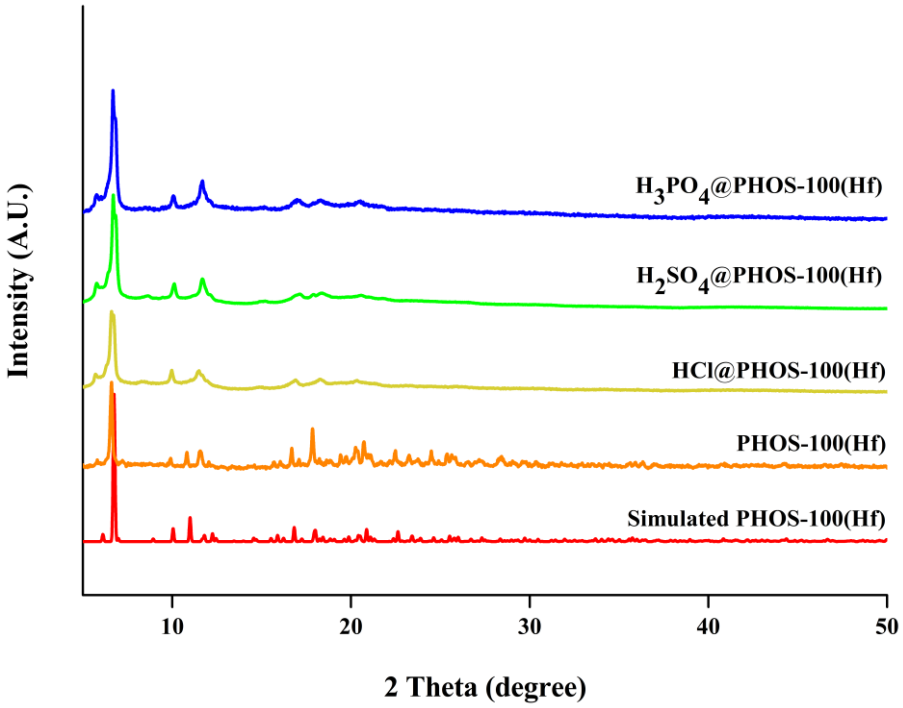

Figure S7. PXRD patterns of samples after activating and loading acidic guest molecules.

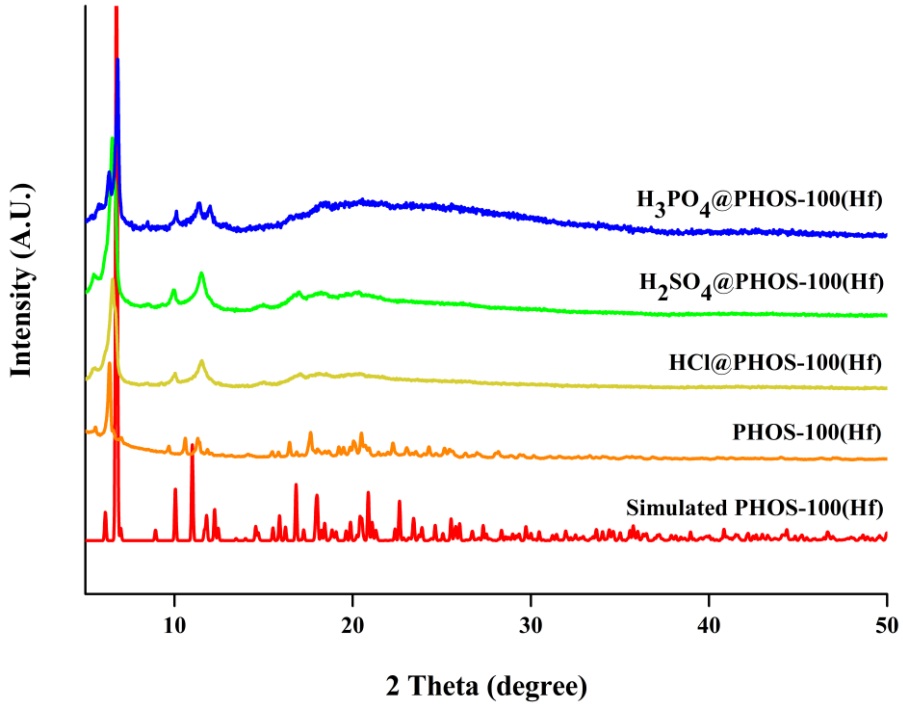

Figure S8. PXRD patterns of samples after water adsorption/desorption measurements recorded at 25 ℃.

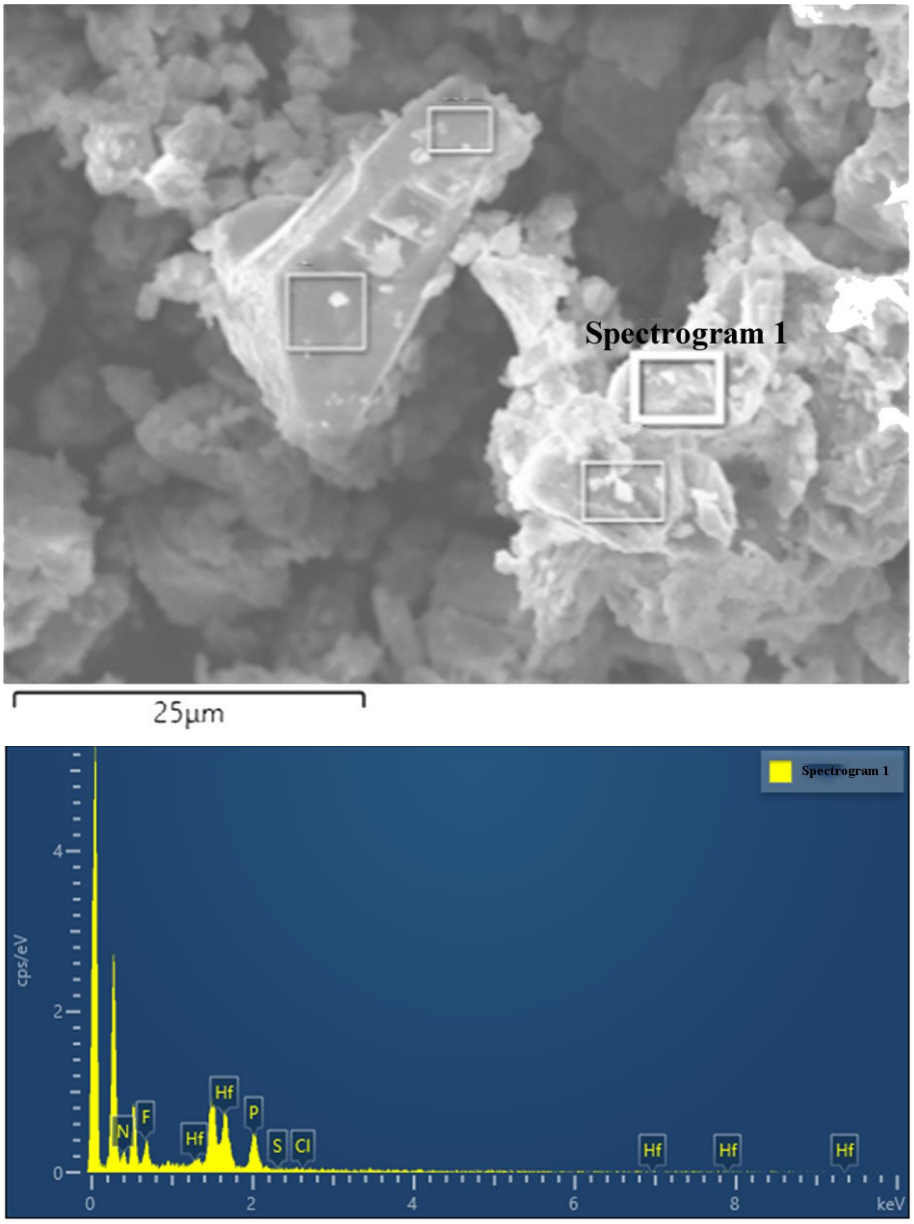

Figure S9. EDS spectrum collected on the marked area of **PHOS-100(Hf)**.

Table S3. Element distribution of **PHOS-100(Hf)**.

Element	Ac %	K-Ratio	Wt %	mol %
N	5.85	0.01041	5.14	16.05
F	26.82	0.05266	16.92	38.90
P	17.44	0.09752	23.04	31.45
S	0.05	0.00045	0.11	0.15
Cl	0.00	0.00000	0.00	0.00
Hf	21.41	0.21414	54.79	13.45

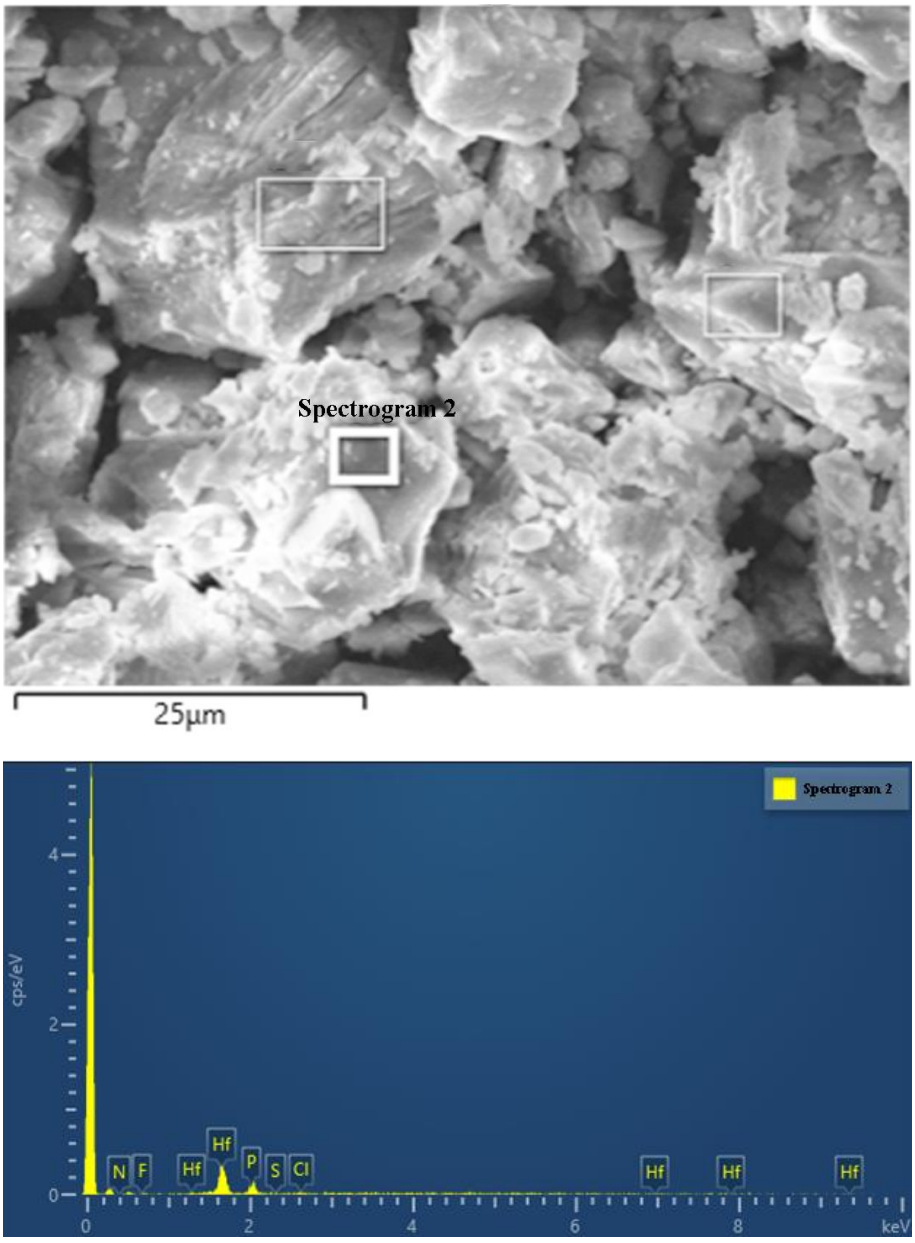

Figure S10. EDS spectrum collected on the marked area of **HCl@PHOS-100(Hf)**.

Table S4. Element distribution of **HCl@PHOS-100(Hf)**.

Element	Ac %	K-Ratio	Wt %	mol %
N	0.00	0.00000	0.00	0.00
F	15.73	0.03088	9.86	31.69
P	23.01	0.12868	21.51	42.37
S	0.00	0.00000	0.00	0.00
Cl	1.19	0.01043	1.78	3.07
Hf	38.99	0.38988	66.85	22.87

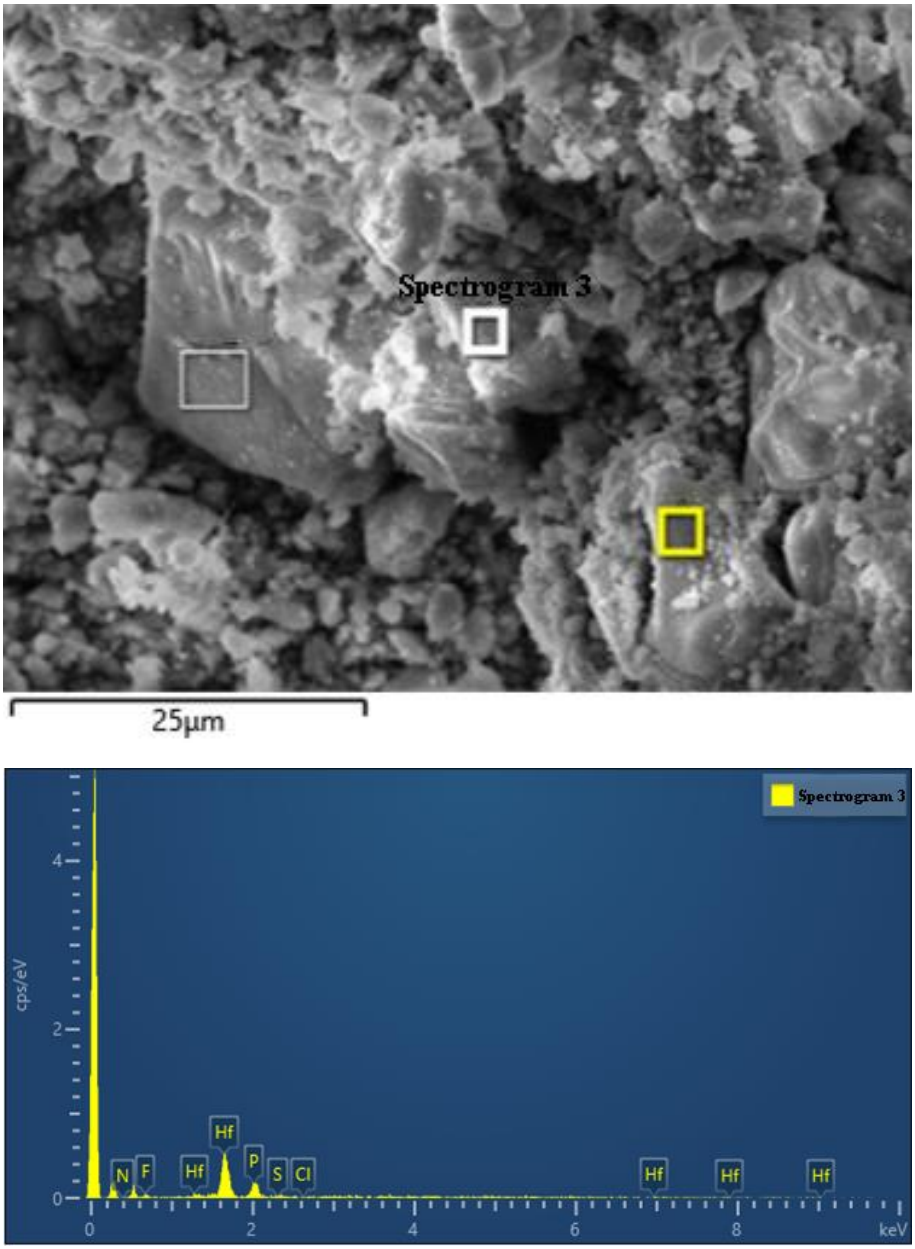

Figure S11. EDS spectrum collected on the marked area of **H_2SO_4@PHOS-100(Hf)**.

Table S5. Element distribution of **H_2SO_4@PHOS-100(Hf)**.

Element	Ac %	K-Ratio	Wt %	mol %
N	0.00	0.00000	0.00	0.00
F	6.98	0.01371	3.95	17.26
P	13.56	0.07584	15.81	42.35
S	0.83	0.00712	1.44	3.73
Cl	0.00	0.00000	0.00	0.00
Hf	38.28	0.38278	78.80	36.66

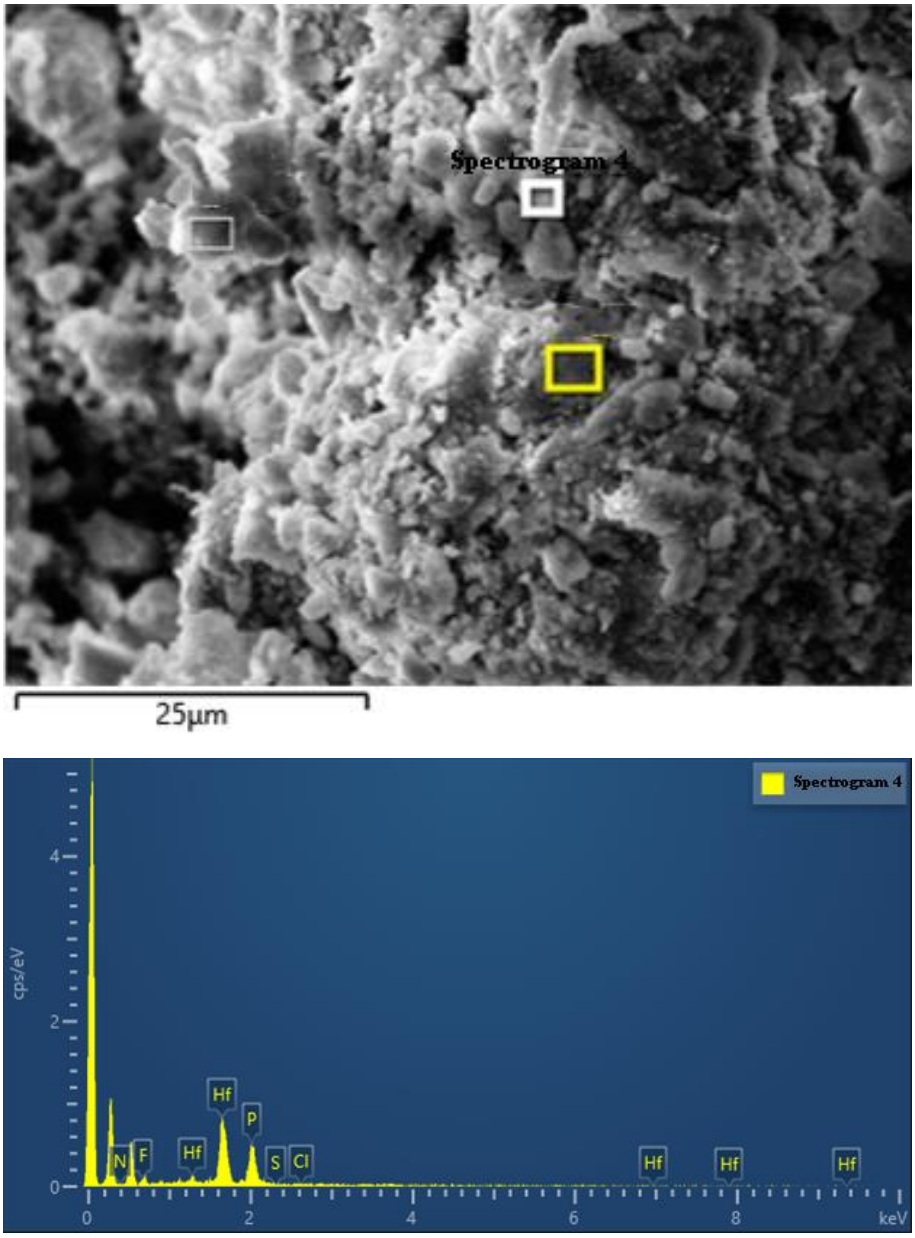

Figure S12. EDS spectrum collected on the marked area of **H_3PO_4@PHOS-100(Hf)**.

Table S6. Element distribution of **H_3PO_4@PHOS-100(Hf)**.

Element	Ac %	K-Ratio	Wt %	mol %
N	0.00	0.00000	0.00	0.00
F	15.18	0.02981	6.63	23.26
P	26.13	0.14616	23.57	50.68
S	0.00	0.00000	0.00	0.00
Cl	0.00	0.00000	0.00	0.00
Hf	42.45	0.42448	69.81	26.06

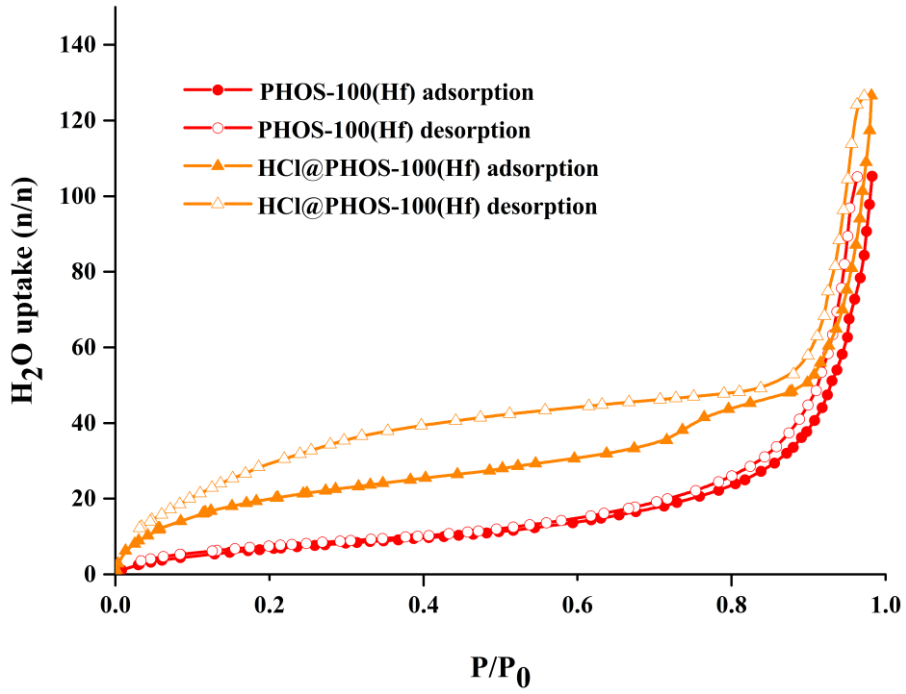

Figure S13. Water adsorption (filled circles) and desorption (open circles) isotherms of **PHOS-100(Hf)** and **HCl@PHOS-100(Hf)** at 25 ℃.

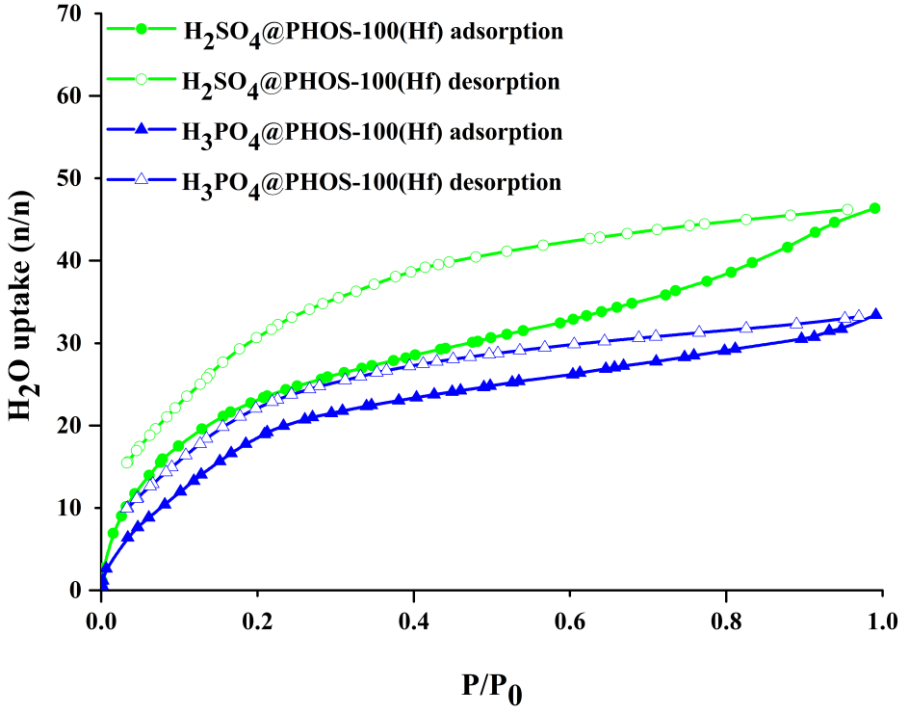

Figure S14. Water adsorption (filled circles) and desorption (open circles) isotherms of **H_2SO_4@PHOS-100(Hf)** and **H_3PO_4@PHOS-100(Hf)** at 25 ℃.

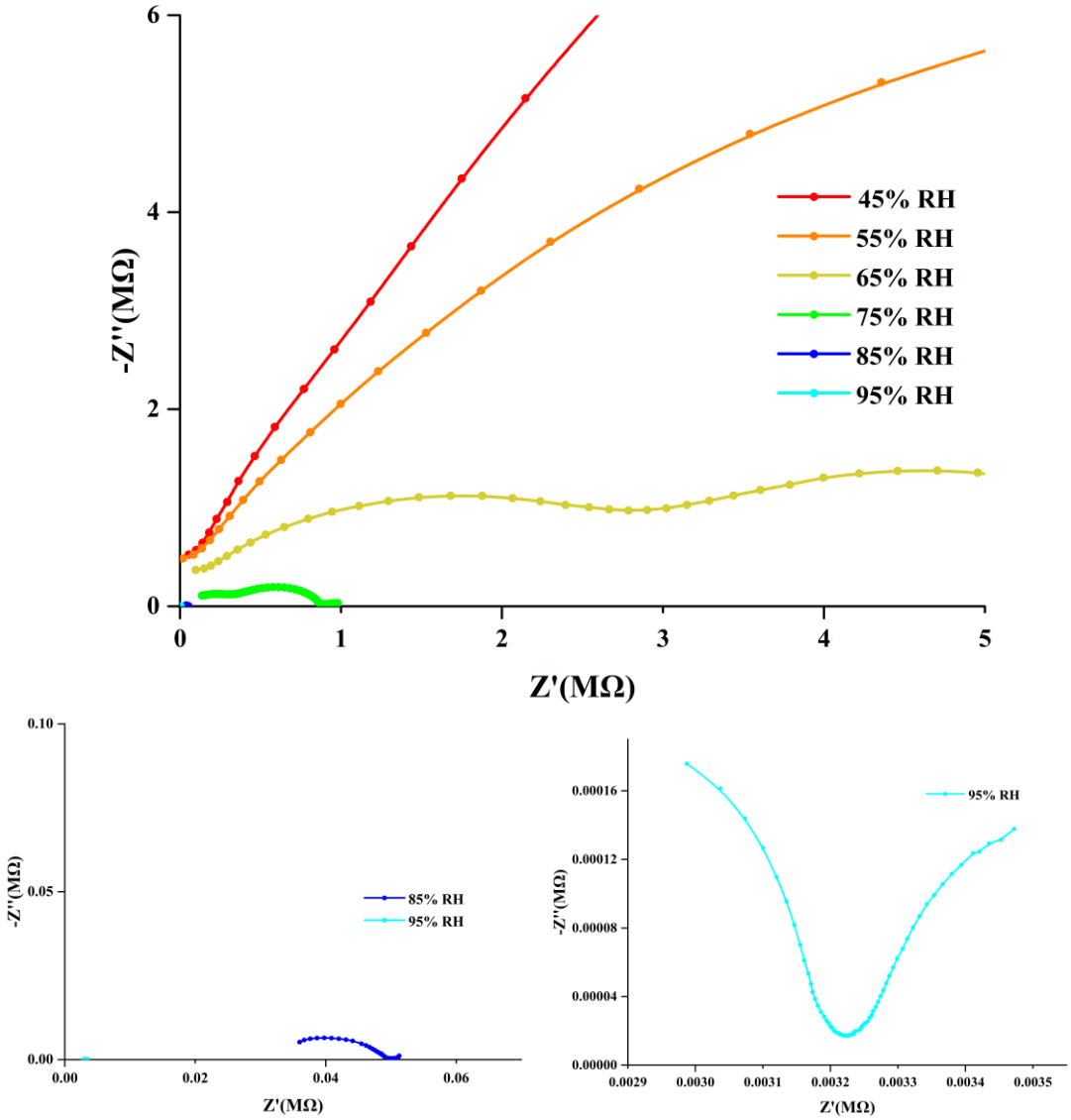

Figure S15. Nyquist plots for the pellet of **PHOS-100(Hf)** at 25 ºC and various RH. Up: RH increases from 45 to 95%.

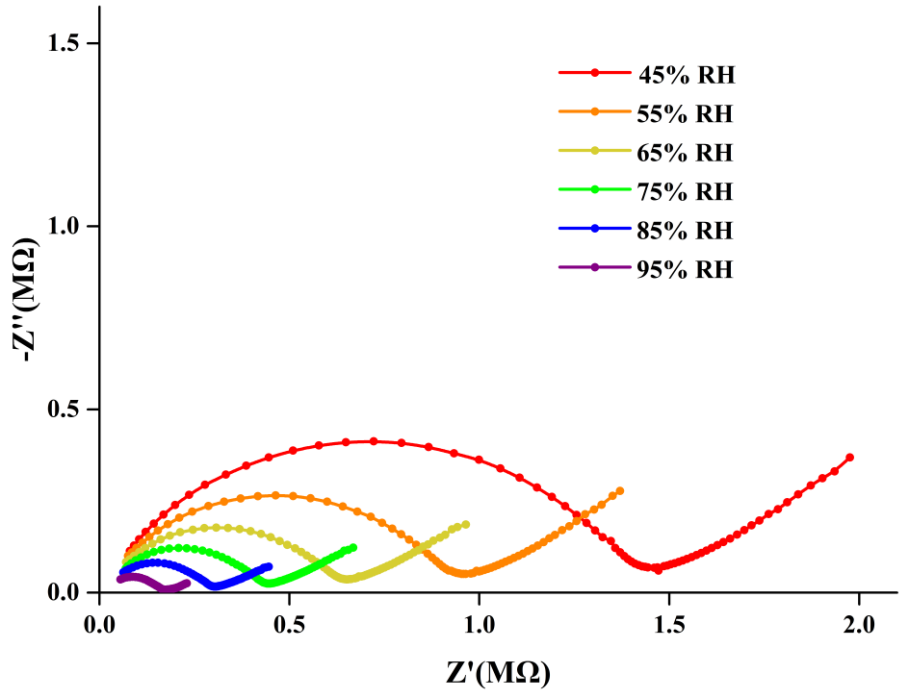

Figure S16. Nyquist plots for the pellet of **HCl@PHOS-100(Hf)** at 25 ºC and various RH. Up: RH increases from 45 to 95%.

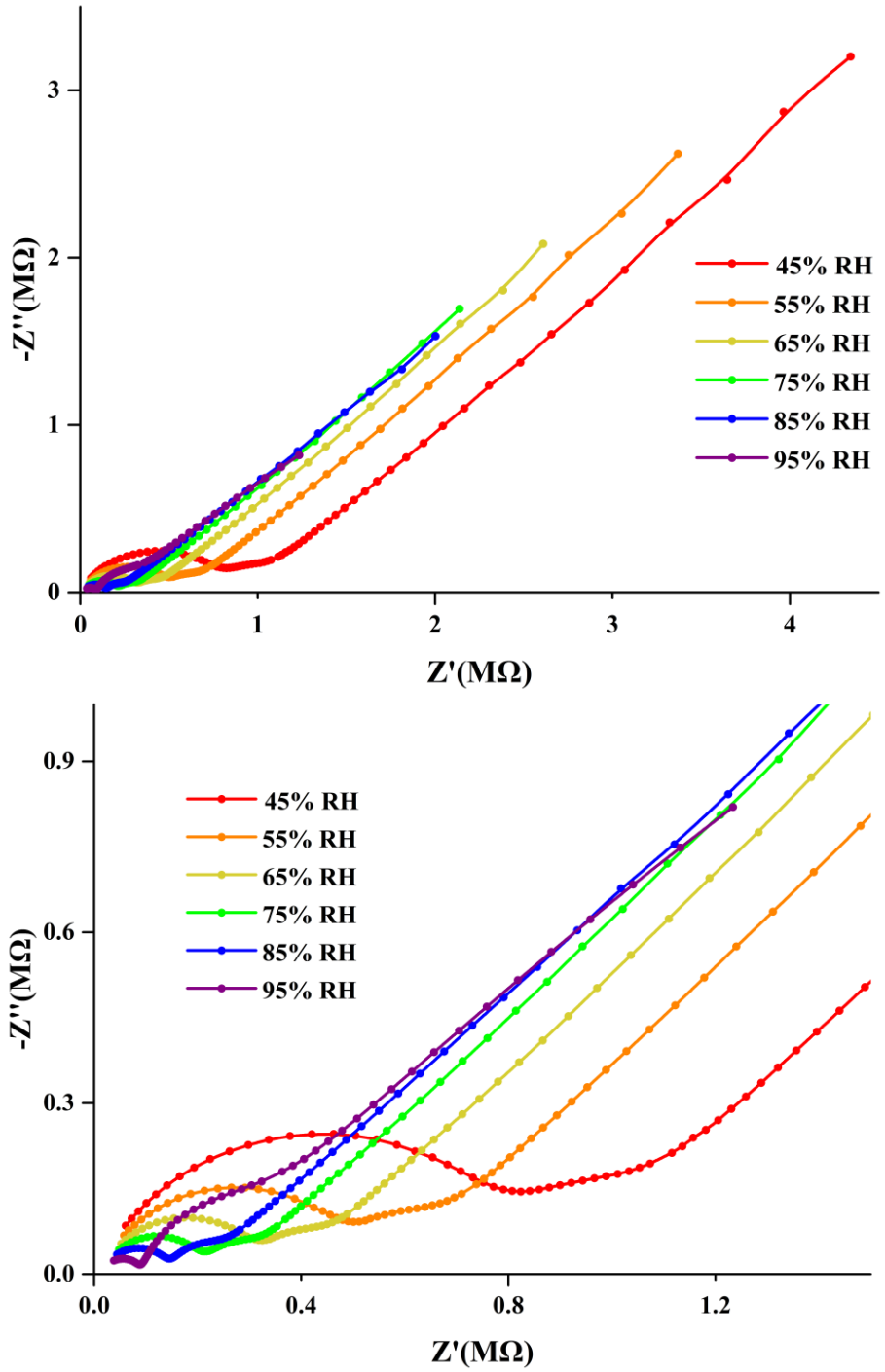

Figure S17. Nyquist plots for the pellet of **H_2SO_4@PHOS-100(Hf)** at 25 °C and various RH. Up: RH increases from 45 to 95%; Down: The enlarged view of graph.

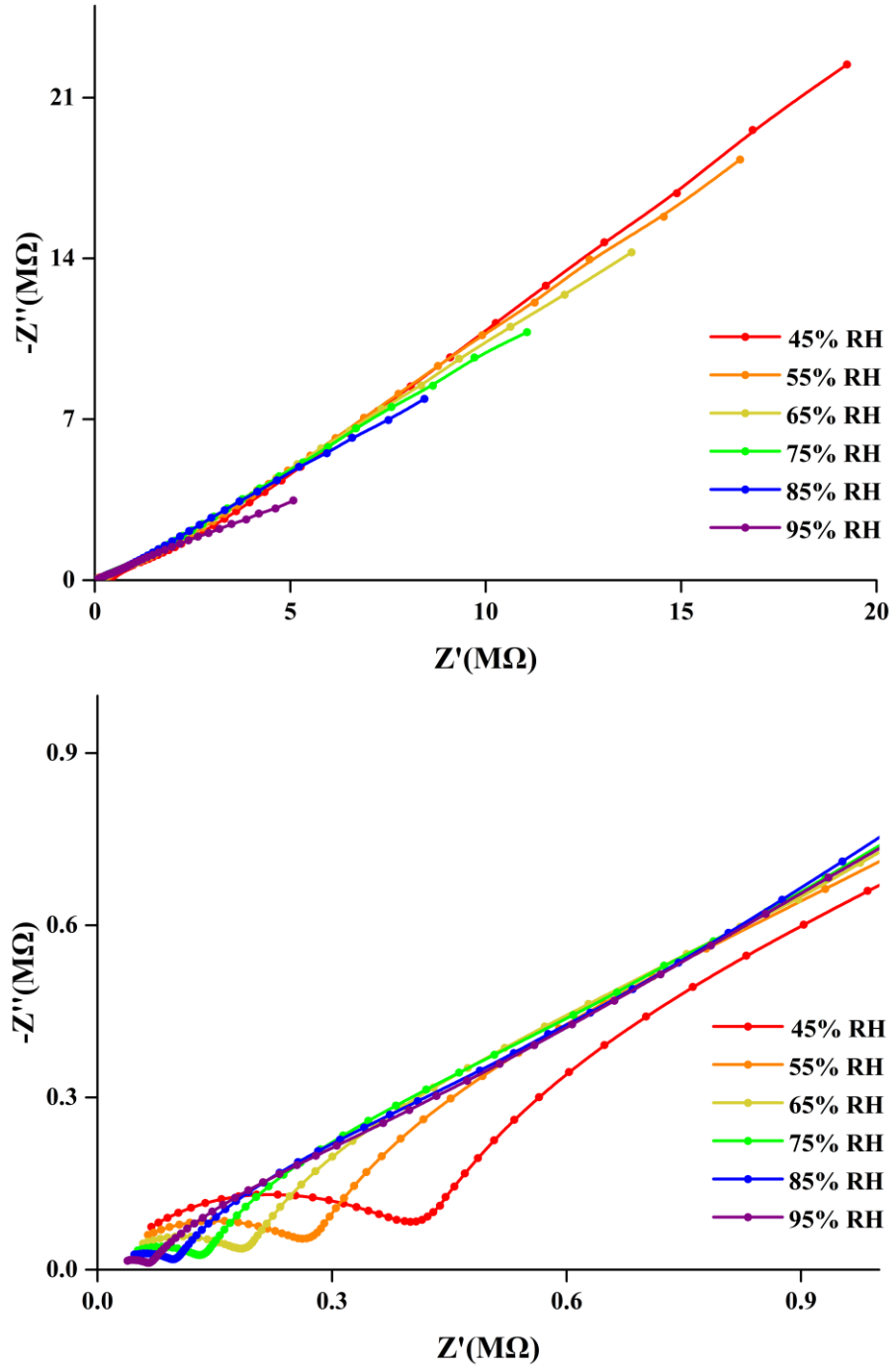

Figure S18. Nyquist plots for the pellet of **H_3PO_4@PHOS-100(Hf)** at 25 °C and various RH. Up: RH increases from 45 to 95%; Down: The enlarged view of graph.

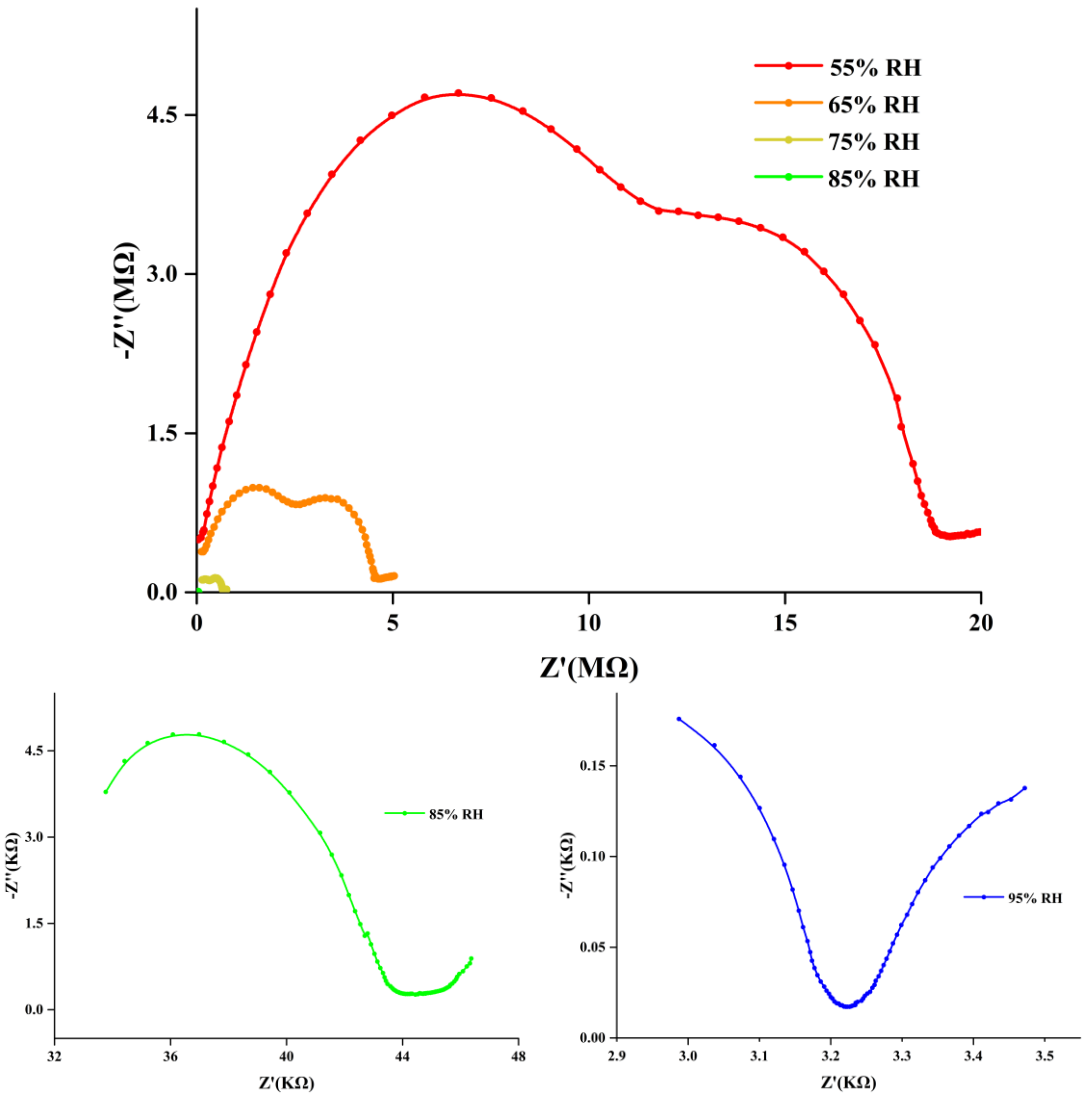

Figure S19. Nyquist plots for the pellet of **PHOS-100(Hf)** at 25 ºC and various RH. Up: RH decreases from 95 to 55%.

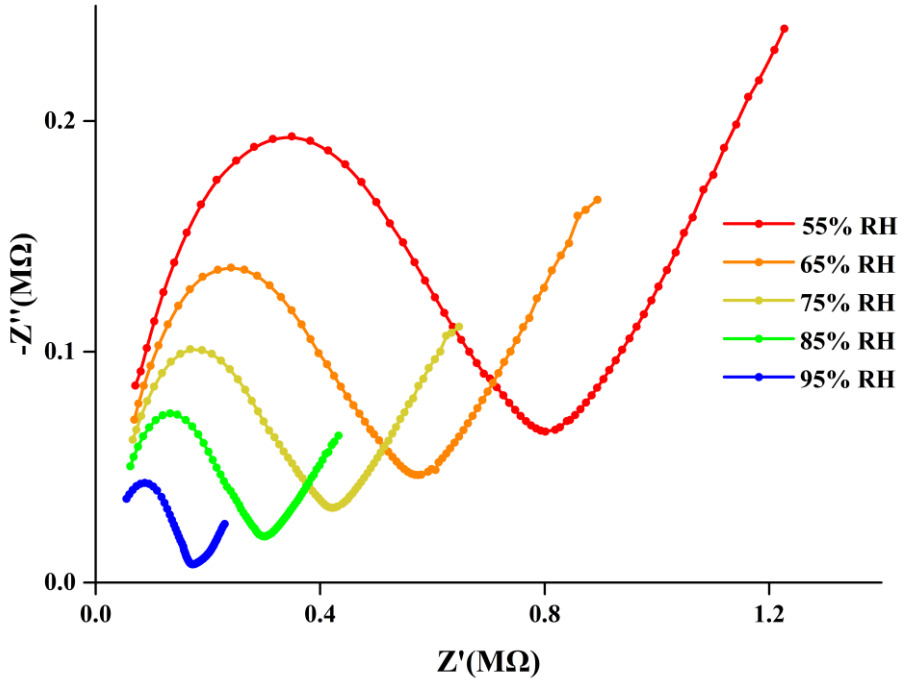

Figure S20. Nyquist plots for the pellet of **HCl@PHOS-100(Hf)** at 25 ºC and various RH. Up: RH decreases from 95 to 55%.

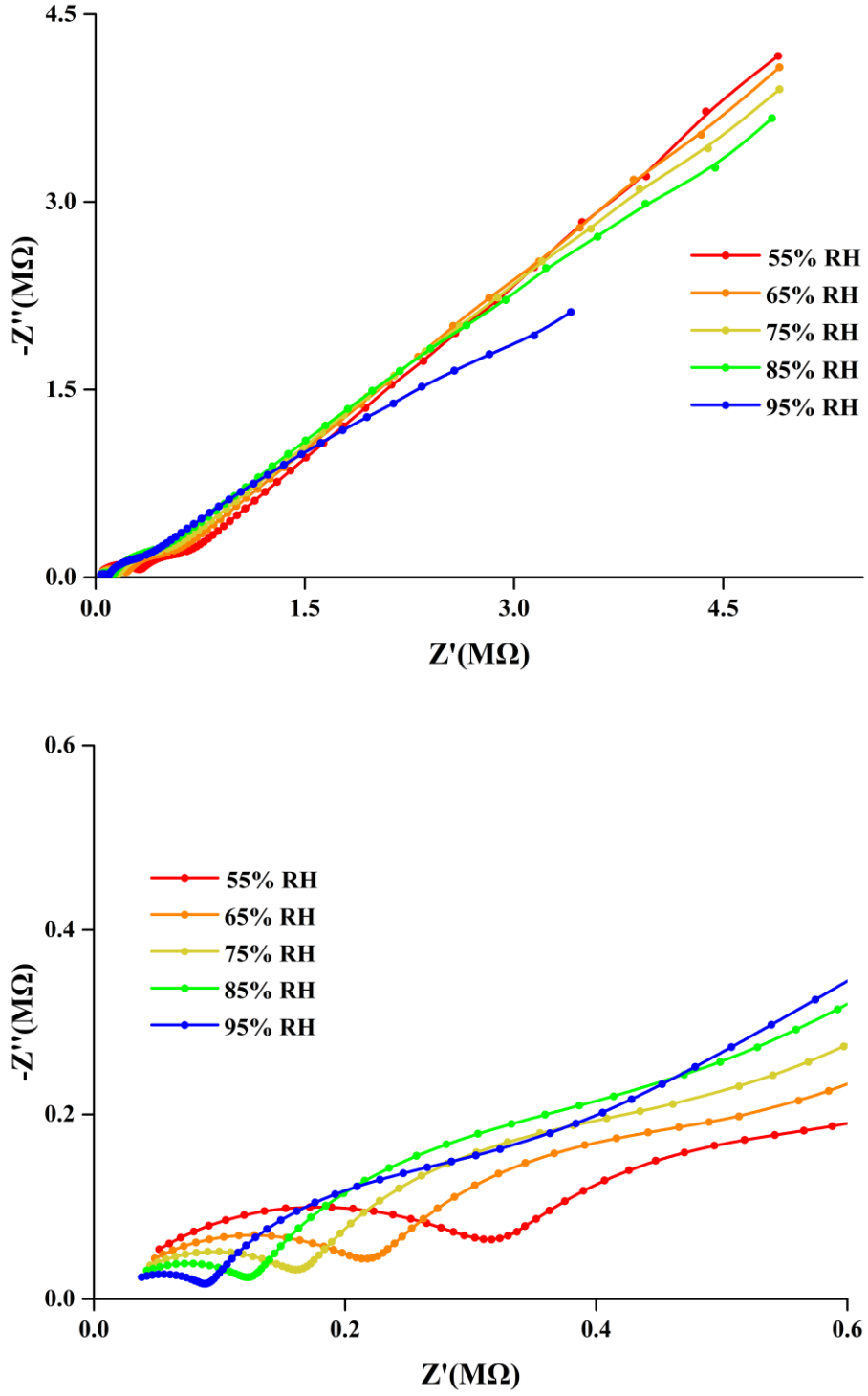

Figure S21. Nyquist plots for the pellet of **H_2SO_4@PHOS-100(Hf)** at 25 ºC and various RH. Up: RH decreases from 95 to 55%; Down: The enlarged view of graph.

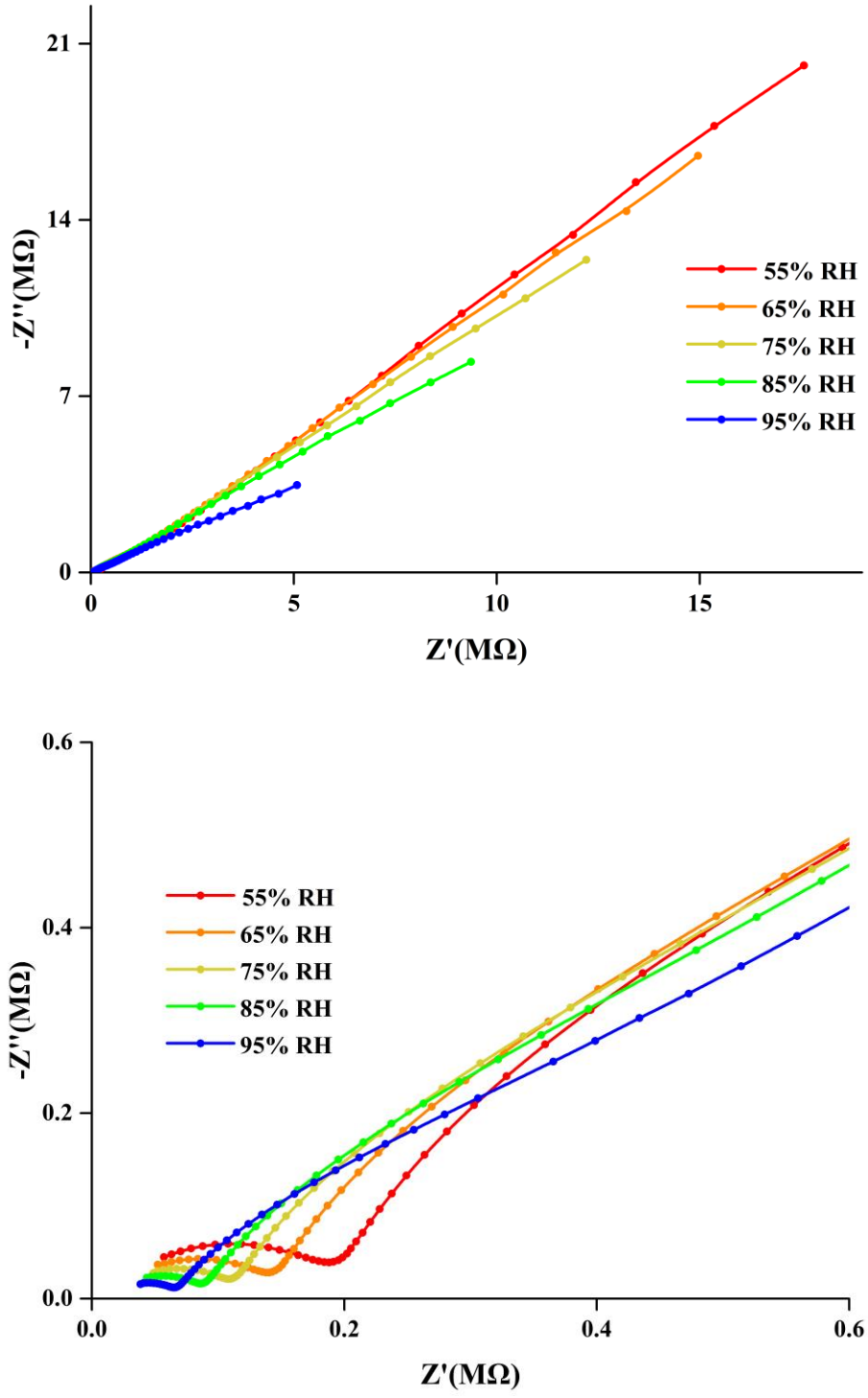

Figure S22. Nyquist plots for the pellet of **H_3PO_4@PHOS-100(Hf)** at 25 °C and various RH. Up: RH decreases from 95 to 55%; Down: The enlarged view of graph.

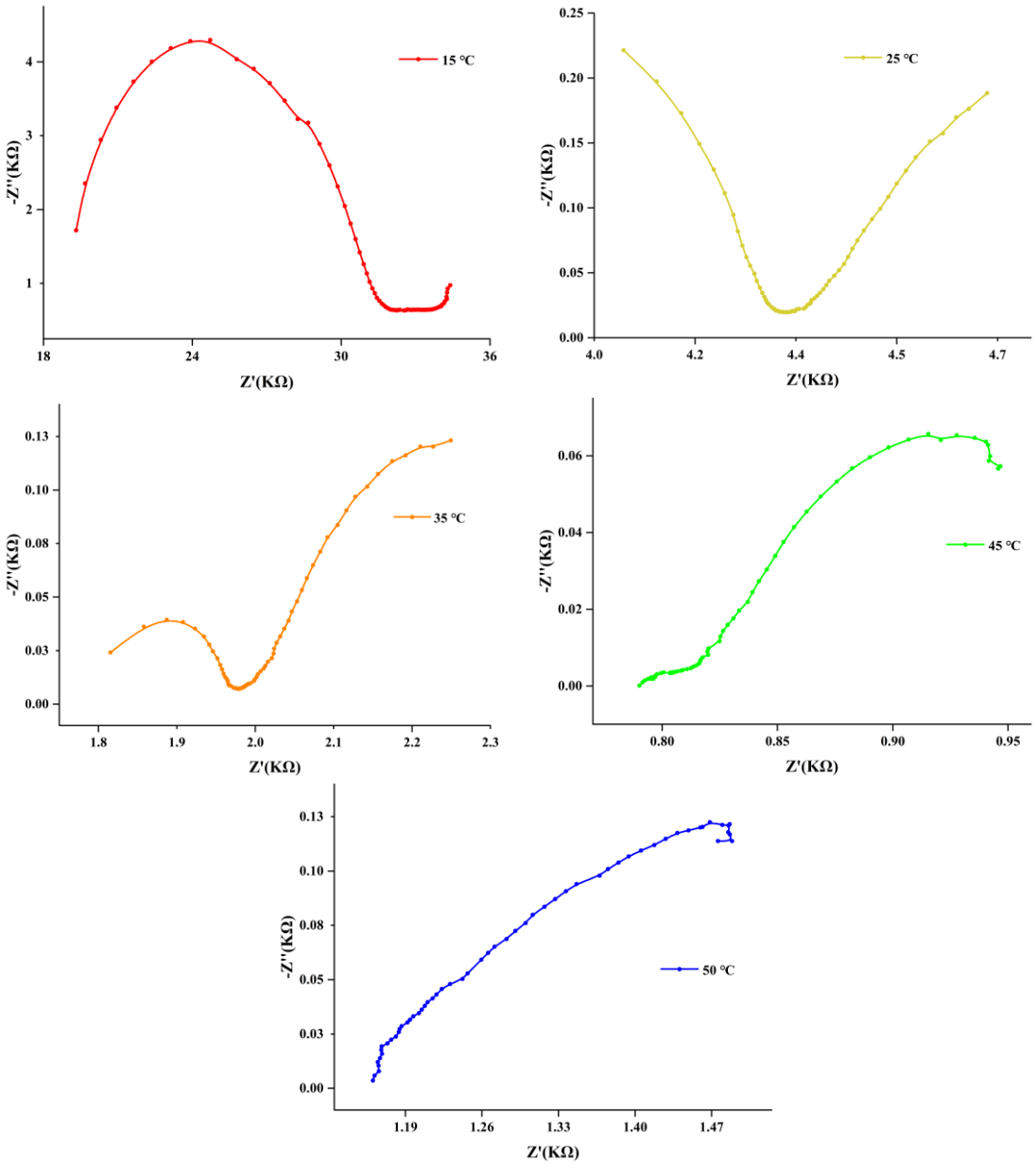

Figure S23. Nyquist plots for **PHOS-100(Hf)** at 95% RH and various temperatures. Up: Temperature increases from 15 to 50 °C.

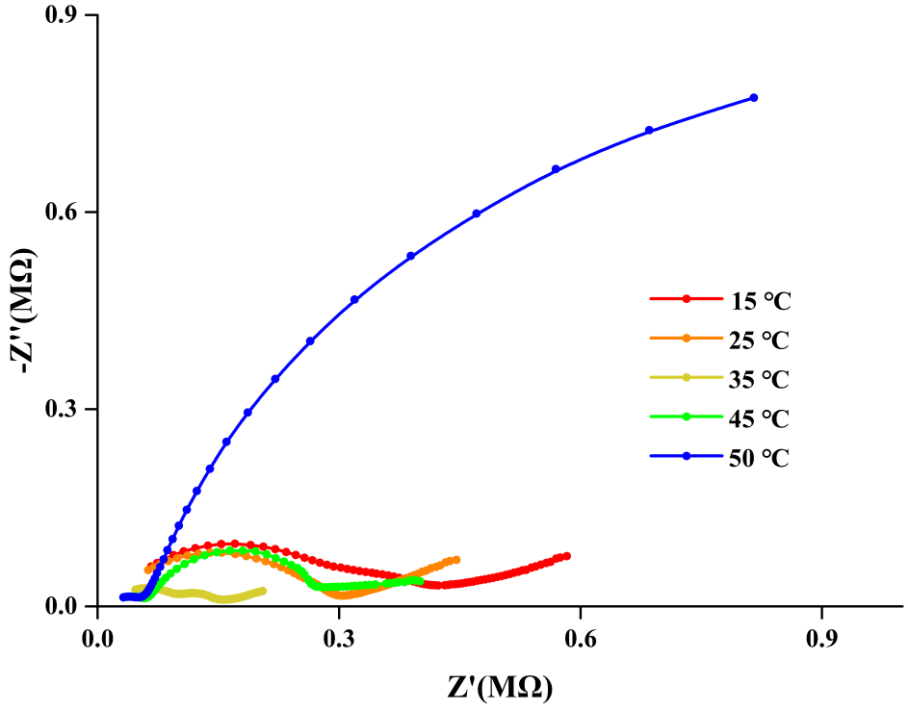

Figure S24. Nyquist plots for **HCl@PHOS-100(Hf)** at 95% RH and various temperatures. Up: Temperature increases from 15 to 50 °C.

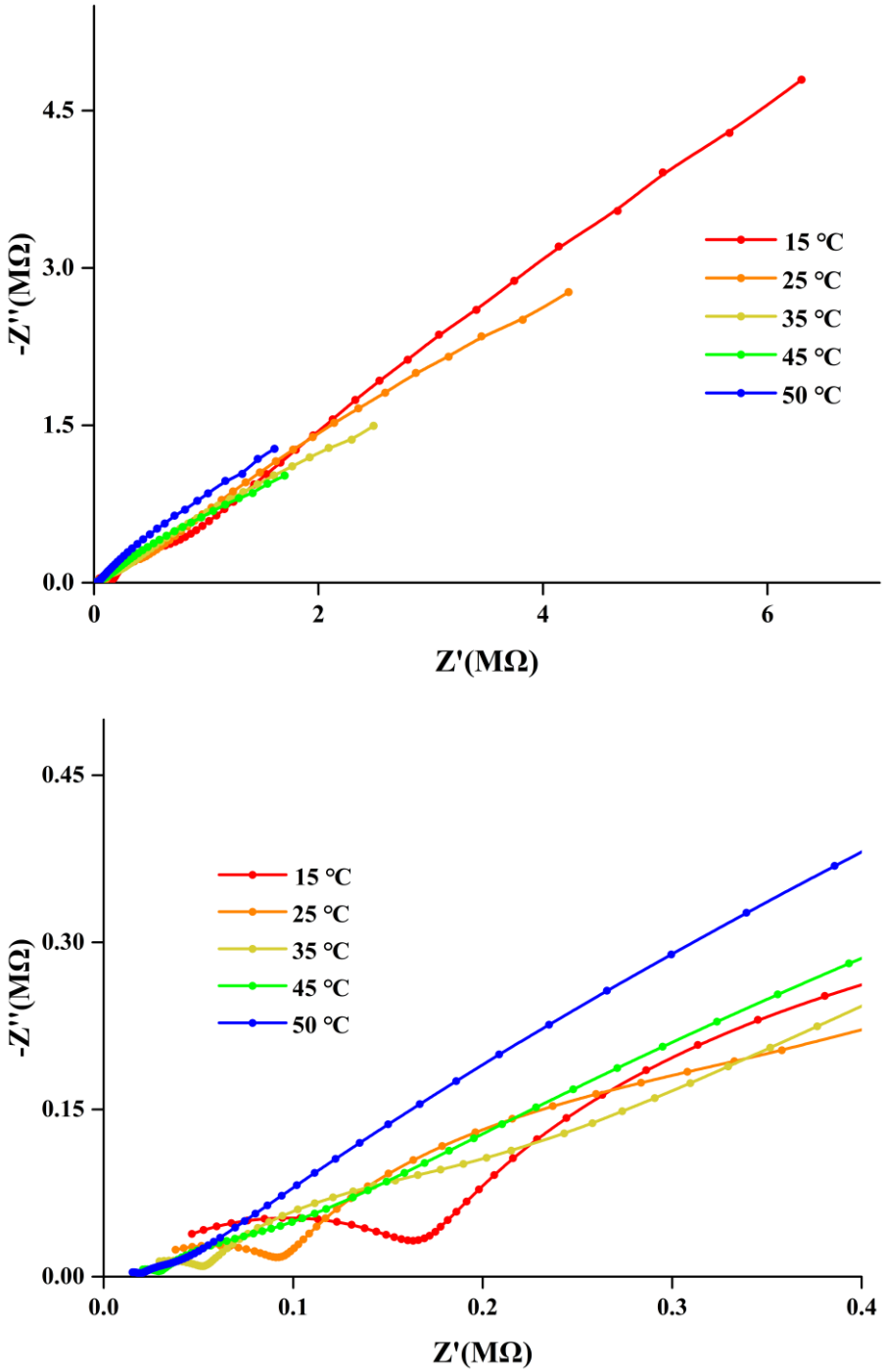

Figure S25. Nyquist plots for **H_2SO_4@PHOS-100(Hf)** at 95% RH and various temperatures. Up: Temperature increases from 15 to 50 ℃; Down: The enlarged view of graph.

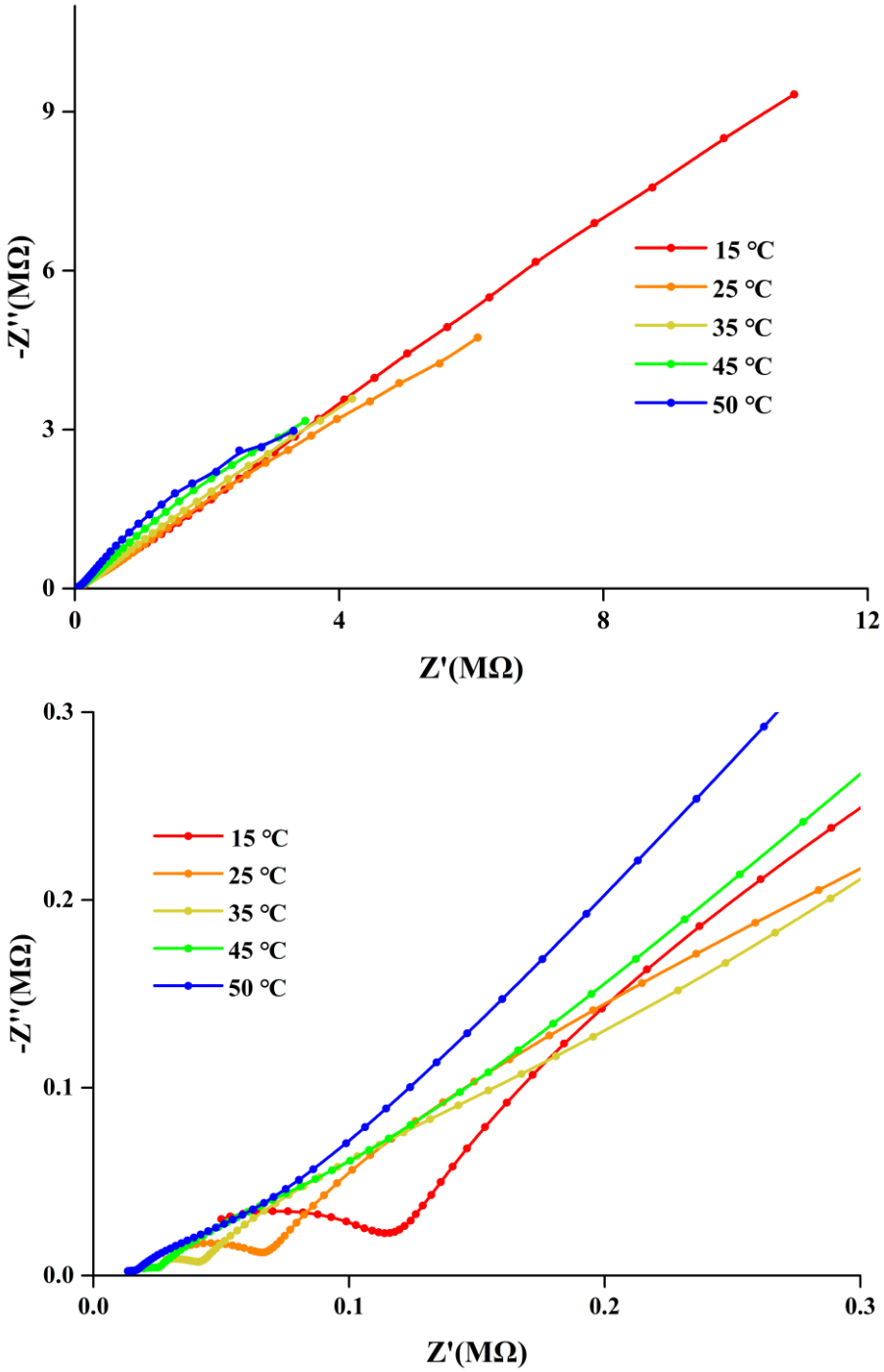

Figure S26. Nyquist plots for **H_3PO_4@PHOS-100(Hf)** at 95% RH and various temperatures. Up: Temperature increases from 15 to 50 °C; Down: The enlarged view of graph.

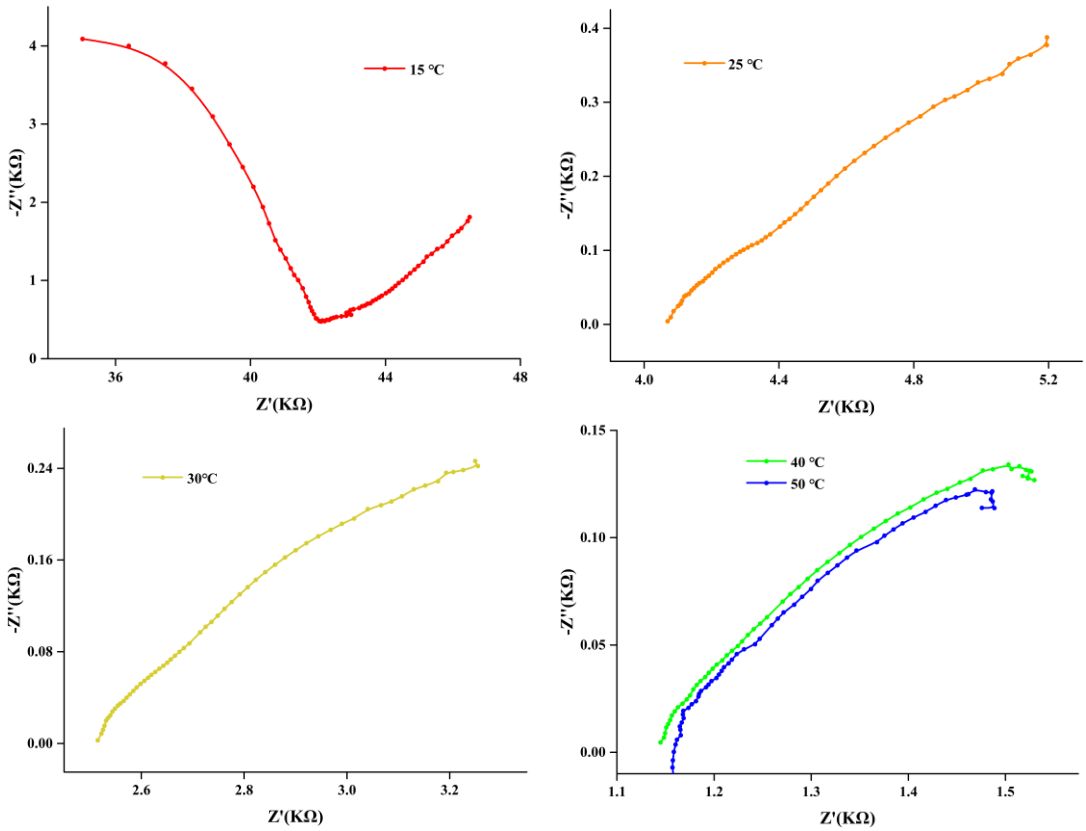

Figure S27. Nyquist plots for **PHOS-100(Hf)** at 95% RH and various temperatures. Up: Temperature decreases from 50 to 15 ℃.

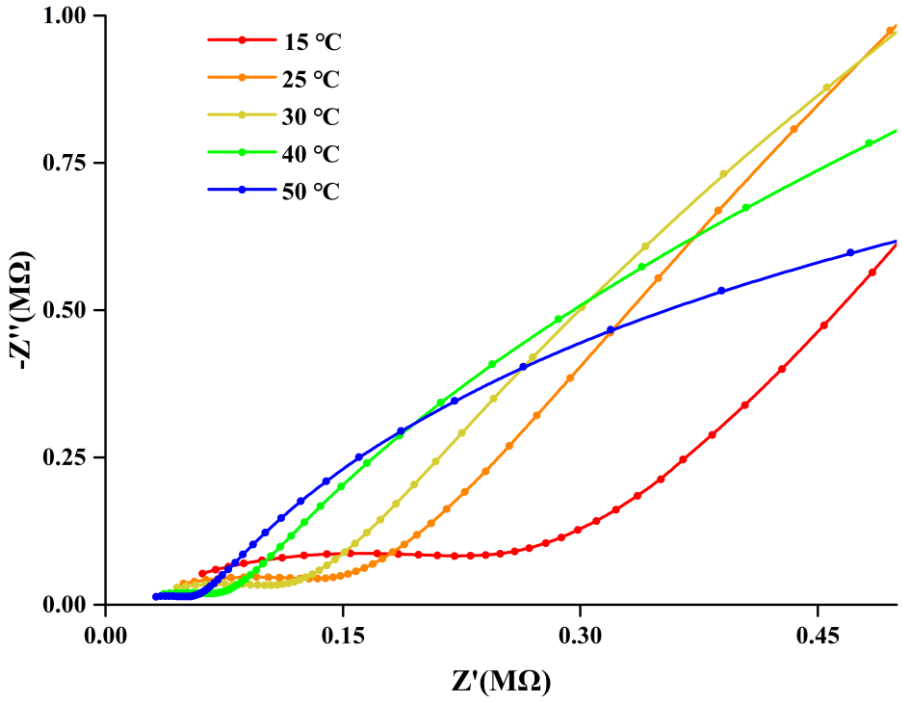

Figure S28. Nyquist plots for **HCl@PHOS-100(Hf)** at 95% RH and various temperatures. Up: Temperature decreases from 50 to 15 ℃.

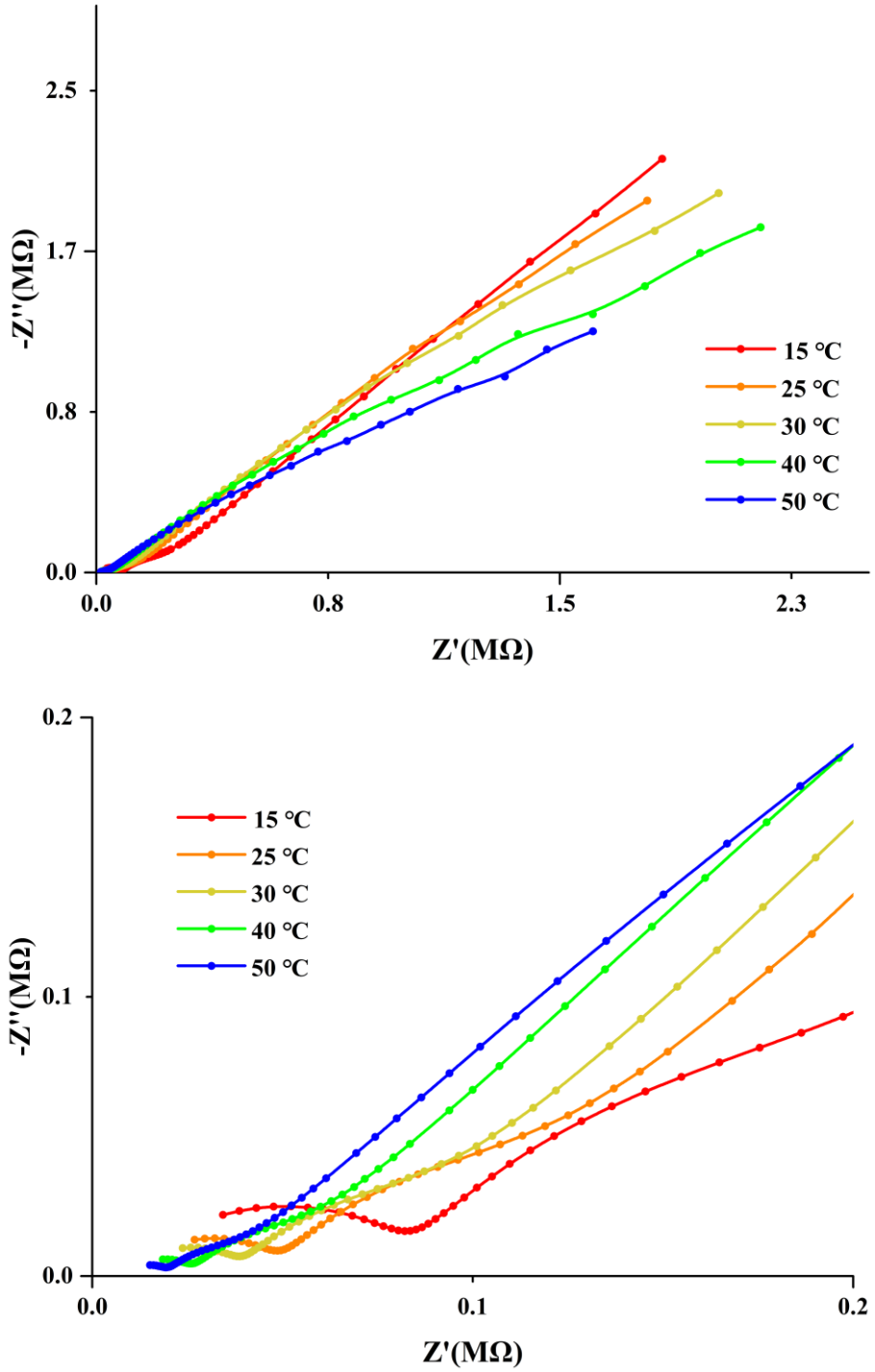

Figure S29. Nyquist plots for **H_2SO_4@PHOS-100(Hf)** at 95% RH and various temperatures. Up: Temperature decreases from 50 to 15 ℃; Down: The enlarged view of graph.

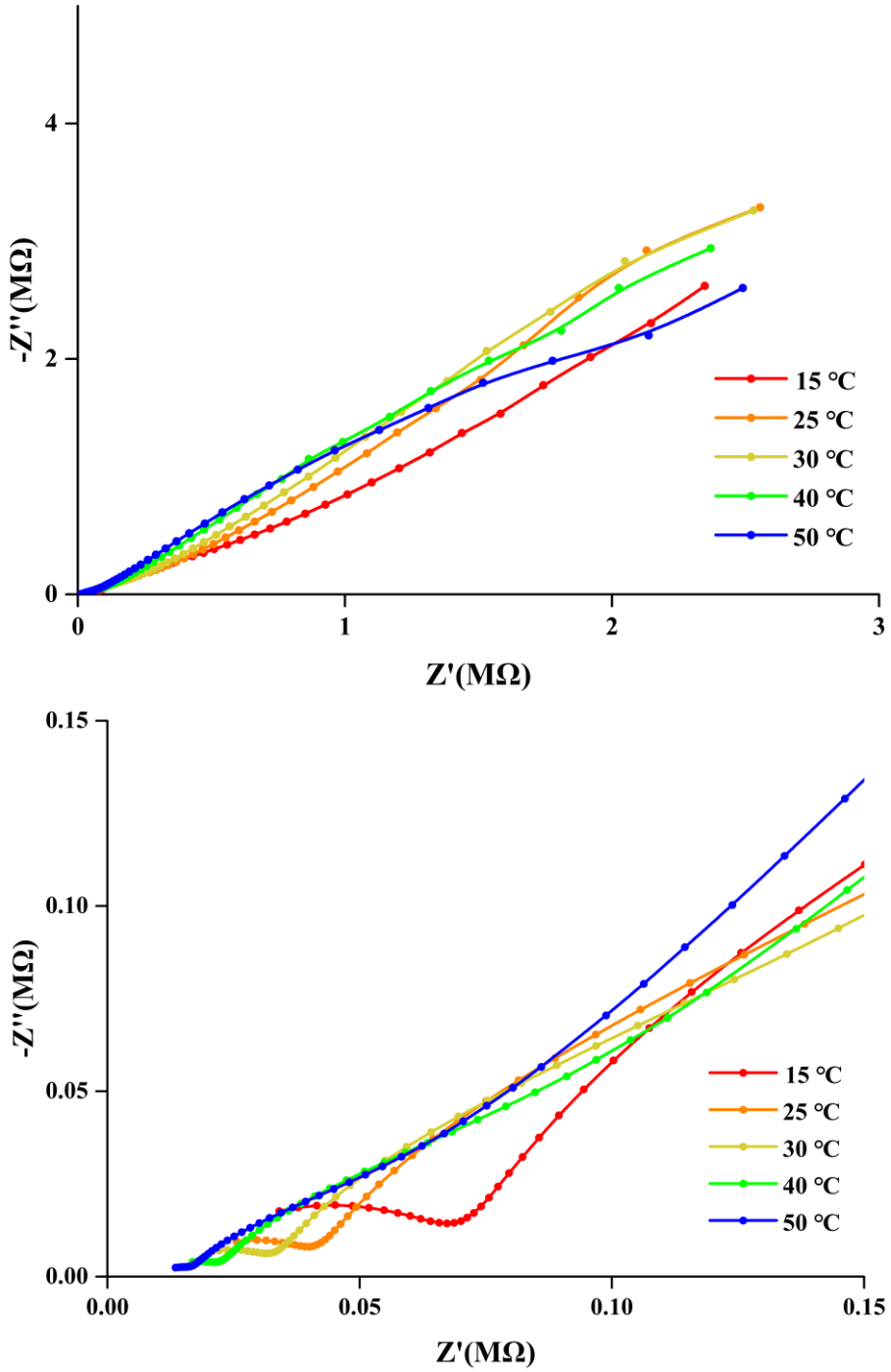

Figure S30. Nyquist plots for **H_3PO_4@PHOS-100(Hf)** at 95% RH and various temperatures. Up: Temperature decreases from 50 to 15 °C; Down: The enlarged view of graph.

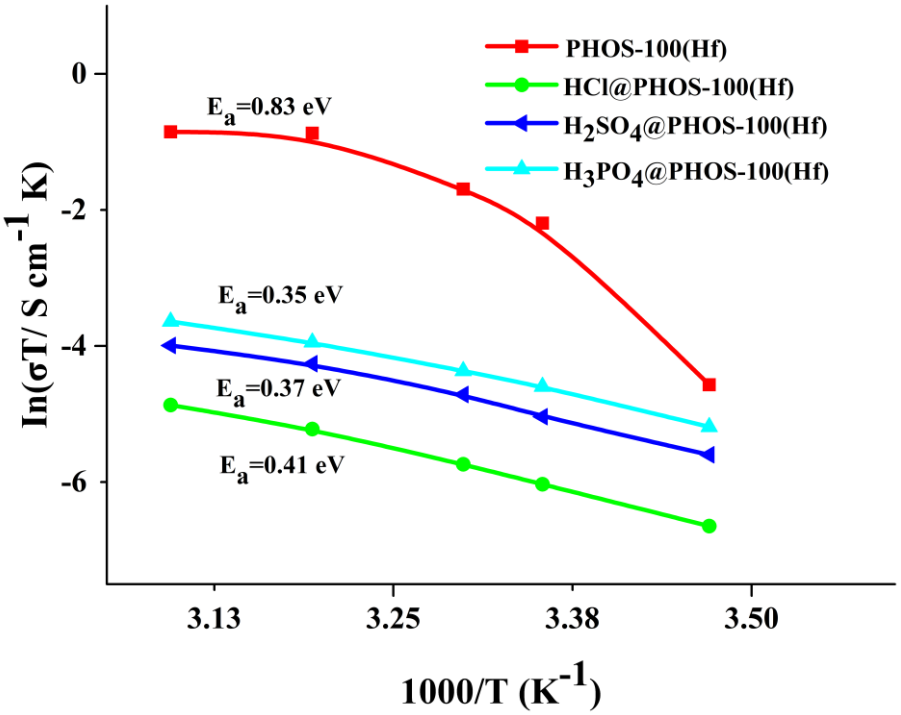

Figure S31. Plots of log (σT) vs. 1000/T for all samples at 95 % relative humidity.

Table S7. Elemental analysis of all samples.

Element ratio / Sample	C	H	N
PHOS-100(Hf)	31.66%	3.86%	3.52%
HCl@PHOS-100(Hf)	26.65%	3.85%	0.39%
H_2SO_4@PHOS-100(Hf)	26.66%	4.17%	0.38%
H_3PO_4@PHOS-100(Hf)	27.94%	3.93%	0.40%

Table S8. Calculation of doped different acidic guest molecules.

	HCl@PHOS-100(Hf)	H_2SO_4@PHOS-100(Hf)	H_3PO_4@PHOS-100(Hf)
n(S/Hf)	0	0.10	
n(P/Hf)	1.85		1.94
Molecules per unit		0.7	0.6

Table S9. Comparison of proton conductivity of **PHOS-100(Hf)** with some other representative MOFs-based proton conductors measured under various condition.

MOFs	Conditions	Before	After	Conditions	Ref
IL@MIL-101	No ionic liquid	1.1×10^{-7}	4.4×10^{-2}	50 ℃ 23 % RH	4
Cr-MIL-88B-PSA	No PSA	6×10^{-3}	1.58×10^{-1}	100 ℃ 85 % RH	5
H_2SO_4 (1 M) @MIL-101(Cr)-NH-$(CH_2)_3SO_3H$	No H_2SO_4	4.8×10^{-3}	1.3×10^{-1}	90 ℃ 95 % RH	6
TEPA@ZIF-8-H_2CO_3	No TEPA	4.5×10^{-6}	2.08×10^{-3}	20 ℃ 99 % RH	7
H_2SO_4@MIL-101-SO_3H	No H_2SO_4	Lower 4 orders of magnitude	1.82	70 ℃ 95 % RH	8
Im@MOF-808	No Im	Lower 1 order of magnitude	3.45×10^{-2}	65 ℃ 99 % RH	9
$[CuI_4CuII_4L_4]_n$-NH_3	No NH_3	4.9×10^{-4}	1.13×10^{-2}	100 ℃ 98 % RH	10
$[Sr(\mu_2\text{-}H_2PhIDC)_2(H_2O)_4]\cdot2H_2O$	water	1.91×10^{-6}	4.76×10^{-2}	90 ℃ 98 % RH ammonia	11
His@VNU-23	No His	1.54×10^{-4}	1.79×10^{-2}	95 ℃ 85 % RH	12
$\{[Co_3(p\text{-}ClPhHIDC)_3(H_2O)_3]\cdot6H_2O\}_n$	No NH_3	2.47×10^{-4}	4.25×10^{-2}	90 ℃ 93 % RH	13
Im@(NENU-3)	Im-Cu@(NENU-3a)	3.16×10^{-4}	1.82×10^{-2}	70 ℃ 90 % RH	14
Im−Fe−MOF	No Im	1.25×10^{-4}	1.21×10^{-2}	60 ℃ 98 % RH	15
Mg(terephthalate)(pyridinol)@Cs^+	No Cs^+	8.3×10^{-6}	1.61×10^{-2}	90 ℃ 90 % RH	16
NH_4Br@HKUST-1	No NH_4Br	1.04×10^{-8}	8.99×10^{-4}	25 ℃ 99 % RH	17

H^+@Ni_2(dobdc)	No H^+	1.4×10^{-4}	2.2×10^{-2}	80 ℃ 95 % RH	[18]

References

1. T. Zheng, Z. Yang, D. Gui, Z. Liu, X. Wang, X. Dai, S. Liu, L. Zhang, Y. Gao, L. Chen, D. Sheng, Y. Wang, J. Diwu, J. Wang, R. Zhou, Z. Chai, T. E. Albrecht-Schmitt and S. Wang, *Nat. Commun.*, 2017, **8**, 15369.
2. G. Sheldrick, *Acta Crystallogr. C.*, 2015, **71**, 3-8.
3. A. Spek, *Acta Crystallogr. C.*, 2015, **71**, 9-18.
4. J. Du, G. Yu, H. Lin, P. Jie, F. Zhang, F. Qu, C. Wen, L. Feng and X. Liang, *J. Colloid Interface Sci.*, 2020, **573**, 360-369.
5. S. S. Liu, Z. Han, J. S. Yang, S. Z. Huang, X. Y. Dong and S. Q. Zang, *Inorg. Chem.*, 2020, **59**, 396-402.
6. S. Devautour-Vinot, E. S. Sanil, A. Geneste, V. Ortiz, P. G. Yot, J. S. Chang and G. Maurin, *Chem Asian J*, 2019, **14**, 3561-3565.
7. Q. Ren, J. W. Yu, H. B. Luo, J. Zhang, L. Wang and X. M. Ren, *Inorg. Chem.*, 2019, **58**, 14693-14700.
8. X.-M. Li, L.-Z. Dong, S.-L. Li, G. Xu, J. Liu, F.-M. Zhang, L.-S. Lu and Y.-Q. Lan, *ACS Energy Lett.*, 2017, **2**, 2313-2318.
9. H.-B. Luo, Q. Ren, P. Wang, J. Zhang, L. Wang and X.-M. Ren, *ACS Appl. Mater. Interfaces*, 2019, **11**, 9164-9171.
10. R. Liu, L. Zhao, S. Yu, X. Liang, Z. Li and G. Li, *Inorg. Chem.*, 2018, **57**, 11560-11568.
11. W. Chen, J. Wang, L. Zhao, W. Dai, Z. Li and G. Li, *J. Alloys Compd.*, 2018, **750**, 895-901.
12. M. V. Nguyen, T. H. N. Lo, L. C. Luu, H. T. T. Nguyen and T. N. Tu, *J. Mater. Chem. A*, 2018, **6**, 1816-1821.
13. X. Liang, B. Li, M. Wang, J. Wang, R. Liu and G. Li, *ACS Appl. Mater. Interfaces*, 2017, **9**, 25082-25086.
14. Y. Ye, W. Guo, L. Wang, Z. Li, Z. Song, J. Chen, Z. Zhang, S. Xiang and B. Chen, *J. Am. Chem. Soc.*, 2017, **139**, 15604-15607.
15. F. M. Zhang, L. Z. Dong, J. S. Qin, W. Guan, J. Liu, S. L. Li, M. Lu, Y. Q. Lan, Z. M. Su and H. C. Zhou, *J. Am. Chem. Soc.*, 2017, **139**, 6183-6189.
16. S. Shalini, S. Aggarwal, S. K. Singh, M. Dutt, T. G. Ajithkumar and R. Vaidhyanathan, *Eur. J. Inorg. Chem.*, 2016, **2016**, 4382-4386.
17. Y.-W. You, C. Xue, Z. Tian and S.-X. Liu, *Dalton Trans.*, 2016, **45**.
18. W. J. Phang, W. R. Lee, K. Yoo, D. W. Ryu, B. Kim and C. S. Hong, *Angew. Chem. Int. Ed.*, 2014, **53**, 8383-8387.